Title

Lipidomic Analysis of Dynamic Eicosanoid Responses during the Induction and Resolution of Lyme Arthritis*

Journal

Journal of Biological Chemistry, 284(32)

ISSN

0021-9258

Authors

Blaho, Victoria A
Buczynski, Matthew W
Brown, Charles R
et al.

Publication Date

2009-08-01

DOI

10.1074/jbc.m109.003822

Peer reviewed

THE JOURNAL OF BIOLOGICAL CHEMISTRY VOL. 284, NO. 32, pp. 21599–21612, August 7, 2009

Lipidomic Analysis of Dynamic Eicosanoid Responses during the Induction and Resolution of Lyme Arthritis*[S]

Received for publication, April 7, 2009, and in revised form, May 28, 2009 Published, JBC Papers in Press, June 1, 2009, DOI 10.1074/jbc.M109.003822

Victoria A. Blaho[‡1], **Matthew W. Buczynski**[§1,2], **Charles R. Brown**[‡3], **and Edward A. Dennis**[§4]

From the [‡]*Department of Veterinary Pathobiology, University of Missouri, Columbia, Missouri 65211 and the* [§]*Department of Pharmacology and Department of Chemistry and Biochemistry, University of California San Diego, La Jolla, California 92093*

Eicosanoids and other bioactive lipid mediators are indispensable regulators of biological processes, as demonstrated by the numerous inflammatory diseases resulting from their dysregulation, including cancer, hyperalgesia, atherosclerosis, and arthritis. Despite their importance, a robust strategy comparable with gene or protein array technology for comprehensively analyzing the eicosanoid metabolome has not been forthcoming. We have developed liquid chromatography-tandem mass spectrometry methodology that quantitatively and comprehensively analyzes the eicosanoid metabolome and utilized this approach to characterize eicosanoid production during experimental Lyme arthritis in mice infected with the bacterium *Borrelia burgdorferi*. Eicosanoids were extracted throughout infection from the joints of Lyme arthritis-resistant and -susceptible mice and subjected to lipidomic profiling. We identified temporal and quantitative differences between these mouse strains in the production of eicosanoids, which correlated with differences in arthritis development. The eicosanoid biosynthetic enzyme cyclooxygenase (COX)-2 has been implicated in the regulation of Lyme arthritis pathology, and subsequent lipidomic profiling of *B. burgdorferi*-infected COX-2$^{-/-}$ mice identified reductions not only in COX-2 products but, surprisingly, also significant off-target reductions in 5-lipoxygenase metabolites. Our results demonstrate the utility of a comprehensive lipidomic approach for identifying potential contributors to disease pathology and may facilitate the development of more precisely targeted treatment strategies.

Systems biology has advanced exponentially during the past decade, producing a wealth of data relating to disease susceptibility and pathology. Because of its immense scope and complex chemical composition, metabolomics has lagged behind its genomics and proteomics counterparts, hampering the advancement of sequential systems biology as a cohesive approach to disease investigation and drug discovery (1). The unique challenges faced by metabolomics researchers are evident in the emerging field of lipidomics, the analysis and characterization of the enormous and diverse set of lipid molecules. For this reason, the Lipid Metabolites and Pathway Strategy (LIPID MAPS) consortium was created to provide an intellectual infrastructure for the advancement of lipidomics (2). To expedite the elevation of lipidomics to a level comparable with that of genomics and proteomics, efforts have included the establishment of a comprehensive lipid classification system (3), the adoption of liquid chromatography-tandem mass spectrometry (LC-MS/MS)[5] as the preferred methodology for lipid analysis (2), and the development of a publicly accessible data base of lipid mass spectra and standards (see Lipidomics Gateway web site). These integrated components provide a springboard for the investigation of potential interactions between large classes of lipid signaling molecules and their impact on the induction and modulation of disease pathology.

Eicosanoids comprise a diverse class of over one hundred bioactive lipid mediators derived from the metabolism of polyunsaturated fatty acids by cyclooxygenase (COX) (4, 5), lipoxygenase (LOX) (4–6), and cytochrome P450 (CYP) (4, 7) as well as other non-enzymatic pathways (4). As a class, these molecules act as spatially localized hormone-like signaling molecules that have a wide range of effects, and under non-disease conditions contribute to the maintenance of homeostasis in almost every organ system (5). However, it is because of their participation in inflammatory diseases that eicosanoids have been the target of intense study. For example, cyclooxygenases can generate pro-inflammatory prostaglandins (PG), which are responsible for many of the hallmark signs of inflammation such as heat, redness, swelling and pain, whereas cytochrome P450s create epoxyeicosatrienoic acids (EET), which may affect local inflammation by promoting vasodilatation, and the lipoxygenases, which generate molecules with diverse signaling effects such as pro-inflammatory leukotrienes (LT) or anti-inflammatory/pro-resolution lipoxins (LX), resolvins (Rv), and protectins (PD). Metabolic and non-enzymatic breakdown

* This work was supported, in whole or in part, by National Institutes of Health LIPID MAPS Large Scale Collaborative Grant GM069338 from NIGMS (to E. A. D.) and National Institutes of Health Grant R01-AR052748 from NIAMS (to C. R. B.).

[S] The on-line version of this article (available at http://www.jbc.org) contains supplemental Figs. S1–S3 and Tables 1–5.

[1] Both authors contributed equally to this work.

[2] Supported in part by National Institutes of Health Gastroenterology Training Grant T32 DK07202.

[3] To whom correspondence may be addressed: University of Missouri, 315 Connaway Hall, Columbia, MO 65211. E-mail: BrownChar@missouri.edu.

[4] To whom correspondence may be addressed: University of California San Diego, 9500 Gilman Dr., La Jolla, CA 92093-0601. E-mail: edennis@ucsd.edu.

[5] The abbreviations used are: LC, liquid chromatography; MS/MS, tandem mass spectrometry; C3H, arthritis-susceptible C3H/HeJ mice; COX, cyclooxygenase; CYP, cytochrome P450; d, day; DBA, arthritis-resistant DBA/2J mice; DHA, docosahexaenoic acid; DHET, dihydroxyeicosatrienoic acid; diHDoHE, dihydroxydocosahexaenoic acid; diHOME, dihydroxyoctadecamonoenoic acid; EET, epoxyeicosatrienoic acid; HDoHE, hydroxydocosahexaenoic acid; HETE, hydroxyeicosatetranoic acid; HODE, hydroxyoctadecadienoic acid; HX, hepoxilin; LOX, lipoxygenase; LT, leukotriene; LX, lipoxin; MRM, multiple reaction monitoring; oxoETE, oxoeicosatetraenoic acid; PD, protectin; PG, prostaglandin; Rv, resolvin; WT, wild-type.

products of these lipids can have significantly altered bioactivity, further complicating our understanding of these intricate pathways.

The currently accepted model of inflammation proposes that both the induction of inflammation and its eventual resolution and return to homeostasis are not passive events but instead are coordinated, orderly processes actively signaled by specific protein and lipid molecules (6). The inflammatory response is the first step in the immune response and is characterized by an influx of innate immune cells, the production of soluble pro-inflammatory mediators, and tissue destruction. Conversely, resolution sees an influx of anti-inflammatory macrophages, pro-resolution lipid production, and tissue remodeling and repair. Although the roles of some individual eicosanoids in inflammation have been well studied, the overall biological significance of how these signals act *in vivo* to properly initiate and resolve inflammation has yet to be fully elucidated. Studies specifically addressing pathway interactions have investigated the connections between PGE_2 and LX signaling in several animal models of autoimmunity (8, 9), and Schmelzer *et al.* (10) have identified *in vivo* changes in prostaglandin signaling following modulation of endogenous EETs. Although these studies have examined isolated sectors of the eicosanoid metabolome, no reported study has comprehensively examined the temporal production of these metabolites. Our understanding of eicosanoid involvement in regulating the response to infection is even more fragmented and has been focused primarily on a few select metabolites (11, 12). Thus, a complete metabolomics approach on a scale comparable with current gene microarray technology is essential to achieve a thorough understanding of the inflammatory and immune responses and to facilitate the design of more effective disease therapies.

To date, lipidomics studies have been capable of measuring, at most, only ~40 eicosanoids, fewer than half of the known eicosanoid species, with a per sample run time of over 50 min (13, 14). Additionally, extraction methods have been limited to primarily soft tissue samples such as lung or brain, excluding the possibility of lipidomic analysis of more complex tissues such as arthritic joints. These constraints create significant impediments toward the general applicability of previous methodology and require considerable technical development when applying them to other biological systems. For this reason, we have developed a protocol for complete eicosanoid extraction from complex tissue combined with a comprehensive LC-MS/MS methodology with a run time of 25 min/sample to identify and quantify 104 unique lipid species, which encompasses about 90% of the known eicosanoid metabolome (4). These advances allow this technique to be robustly applied to diverse biological samples at a systems biology level.

To demonstrate the applicability of such an approach, we utilized this strategy to investigate the role of eicosanoids in regulating the development and resolution of arthritis pathology in mice infected with *Borrelia burgdorferi,* the causative agent of Lyme disease. Lyme disease is the most common vector-borne disease in the Northern hemisphere and presents diverse pathologies, the most common of which is arthritis (15). Lyme arthritis manifests in about 60–80% of individuals not treated with antibiotics and is characterized by cellular infiltrate consisting of primarily neutrophils and macrophages, a pathology that is recapitulated in the murine model (16). The resolution of arthritis is thought to be dependent upon the clearance of *B. burgdorferi* from the joints by specific antibodies. Genomic profiling of mouse strains that are resistant (C57BL/6, DBA/2) or susceptible (C3H/He) to the development of Lyme arthritis has yielded intriguing data (17) but has generated more questions than answers as to the determining factor(s) for arthritis development. Although previous studies indicate that eicosanoids may play a role in regulating Lyme arthritis pathology, it is unknown which eicosanoids are involved or what their specific roles might be in this pathology (11).

Here we present the first comprehensive lipidomic analysis of an *in vivo* inflammatory response, from initiation to resolution. Analysis of joints from Lyme arthritis-resistant and -susceptible mouse strains revealed significant differences in basal and infection-induced eicosanoid production between the two strains. We further demonstrate the utility of this approach by performing lipidomic analysis on joints from COX-2-deficient ($COX\text{-}2^{-/-}$) animals during infection with *B. burgdorferi* at the peak of the inflammatory response. Lipidomics of $COX\text{-}2^{-/-}$ joints exhibited the expected decrease in COX-2 products but also revealed surprising decreases in multiple products from the 5-LOX pathway. These data establish the robustness of this protocol, as well as its potential to uncover unexpected regulatory pathways.

EXPERIMENTAL PROCEDURES

Materials—LC grade solvents were purchased from EMD Biosciences (San Diego, CA). Synergy C18 reverse phase high pressure liquid chromatography (HPLC) column and Strata-X solid phase extraction columns were purchased from Phenomenex (Torrance, CA). Eicosanoids were purchased from Cayman Chemicals (Ann Arbor, MI) and Biomol (Plymouth Meeting, PA). With the exception of dihomo-$PGF_{2\alpha}$, primary standards for dihomo (adrenic acid-derived)-prostaglandins were not commercially available; these metabolites were analyzed qualitatively using previously characterized extracts from RAW264.7 murine macrophage cells prepared as described (18).

Animals—Female C3H/HeJ (C3H) and DBA/2J (DBA) mice, 4–6 weeks of age, were purchased from The Jackson Laboratory (Bar Harbor, ME). COX-2 heterozygous mice (B6;129S7-*Ptgs2*^{tm1Jed}) were purchased as breeders from The Jackson Laboratory and backcrossed onto the C3H genetic background for 10 generations. Heterozygous mice were then intercrossed to produce knock-out and wild-type littermates. Animals were housed in a specific pathogen-free facility and given sterile food and water *ad libitum*. All studies were conducted in accordance with the Animal Care and Use Committee of the University of Missouri.

Bacteria and Infections—A virulent, low passage, clonal isolate of the *B. burgdorferi* N40 strain was used for all infections. Frozen stocks were placed in 7.5 ml of Barbour, Stoenner, Kelly (BSK) II medium (Sigma-Aldrich) with 6% rabbit serum (Sigma-Aldrich) and grown to log phase by incubation for 5–6 days at 32 °C. Spirochetes were enumerated using dark field micros-

copy and a Petroff-Hausser counting chamber (Hausser Scientific, Horsham, PA). Spirochete dilutions were made in sterile BSK II medium, and mice were inoculated in both hind footpads with 5×10^4 *B. burgdorferi* organisms in 50 μl of medium for a final inoculum of 1×10^5, a concentration that reliably produces arthritis in susceptible animals (19). Sham-infected control animals were injected with 50 μl of BSK II medium/hind footpad.

Arthritis Severity Scores—To determine arthritis severity scores, a histologic analysis of the left tibiotarsal joint from each mouse was performed following sacrifice. The tibiotarsal joint was excised, fixed in 10% buffered zinc-formalin, and embedded in paraffin, and 5-μm sections were stained with hematoxylin and eosin. The sections were evaluated in a blind manner by two independent observers and were assessed for arthritis severity on a scale of 0 to 4. A score of 0 indicated normal tissue, 1, 2, and 3 indicated minimal, mild, and moderate inflammation, respectively, and 4 indicated severe arthritis. The pathology present in histologic sections was characterized by neutrophil and monocyte infiltration into the joints, tendons, and ligament sheaths; hypertrophy and hyperplasia of the synovium; and fibrin exudates. The extent of the observed inflammatory changes formed the basis for the arthritis severity scores.

Determination of Antibody Levels—*B. burgdorferi*-specific IgM and IgG levels in the sera of infected animals were determined by enzyme-linked immunosorbent assay as described previously (11).

Determination of B. burgdorferi Loads—All tissues were snap-frozen in liquid nitrogen immediately after collection and then stored at −80 °C until extraction. Tissues were homogenized in TRIzol (Invitrogen), and DNA was extracted according to the manufacturer's instructions. Multiplex quantitative PCR for determination of *B. burgdorferi* loads was performed using TaqMan Universal PCR Master Mix (Applied Biosystems, Foster City, CA) as described previously (19). Bacterial loads are expressed as copies of *B. burgdorferi* flagellin per 1000 copies of mouse nidogen.

Eicosanoid Extraction from Tibiotarsal Tissue—Tissues were snap-frozen in liquid nitrogen and stored at −80 °C until extraction. The extraction protocol is a modification of Chen *et al.* (20). For extraction, each frozen tibiotarsal joint was wrapped in foil and placed in liquid nitrogen. The joint was then pulverized and the resulting frozen powder placed immediately in 3 ml of ice-cold 50% ethanol and then weighed. This protocol resulted in a nominal loss of tissue; the weight was later used for the normalization of eicosanoid levels in each sample. 10 μl of antioxidant mixture (0.2 mg/ml butylated hydroxytoluene, 0.2 mg/ml EDTA, 2 mg/ml triphenylphosphine, 2 mg/ml indomethacin in a solution of 2:1:1 methanol:ethanol:H_2O) was added to each sample, and all tubes were kept on ice until incubation at −20 °C for 72 h. Samples were then centrifuged at $3500 \times g$ for 30 min, and the clear ethanolic supernatant was removed to a new tube and dried under nitrogen gas. Samples were reconstituted with 2 ml of 10% MeOH and supplemented with 50 μl of internal standard containing the following deuterated eicosanoids (50 pg/μl, 2.5 ng total): (d_4) 6k $PGF_{1\alpha}$, (d_4) TXB_2, (d_4) $PGF_{2\alpha}$, (d_4) PGE_2, (d_4) PGD_2, (d_4) 15d PGJ_2, (d_{11}) 5-iso $PGF_{2\alpha}$ VI, (d_4) dhk $PGF_{2\alpha}$, (d_4) dhk PGD_2, (d_4) LTB_4, (d_8) 5-hydroxyeicosatetranoic acid (HETE), (d_8) 15-HETE, (d_6) 20-HETE, (d_4) 9-HODE, (d_4) 13-HODE, (d_7) 5-oxoETE, (d_8) 8,9-EET, (d_8) 11,12-EET, (d_8) 14,15-EET, (d_4) 9,10-diHOME, and (d_4) 12,13-diHOME. Samples were sonicated for 30 s with a probe sonicator and purified by solid phase extraction as described previously (21, 22). Prior to LC-MS/MS analysis, samples were evaporated using a SpeedVac and reconstituted in 50 μl of LC solvent A (water-acetonitrile-acetic acid (70:30:0.02, v/v/v)).

Liquid Chromatography and Mass Spectrometry—Eicosanoids were separated by reverse-phase LC on a Synergy C18 column (2.1 × 250 mm) at a flow rate of 300 μl/min at 50 °C. The column was equilibrated in solvent A (water-acetonitrile-acetic acid (70:30:0.02; v/v/v)), and 40 μl of sample (80%) was injected using a 50-μl injection loop and eluted with 0% solvent B (acetonitrile-isopropyl alcohol (50:50, v/v)) between 0 and 1 min. Solvent B was increased in a linear gradient to 25% solvent B until 3 min, to 45% until 11 min, to 60% until 13 min, to 75% until 18 min, and to 90% until 18.5 min. Solvent B was held at 90% until 20 min, dropped to 0% by 21 min, and held until 25 min. Eicosanoids were analyzed using a tandem quadrupole mass spectrometer (ABI 4000 Q-Trap®, Applied Biosystems) via multiple reaction monitoring (MRM) in negative ion mode. The electrospray voltage was −4.5 kV, and the turbo ion spray source temperature was 525 °C. Collisional activation of eicosanoid precursor ions used nitrogen as a collision gas. Eicosanoids were measured using precursor→product (MRM) pairs, and the MS analysis was divided into six periods (Fig. 1, supplemental Table 1). The duty cycle for each period ranged between 390 and 840 ms, with an average time of 565 ms. The declustering potential and collision energy for each eicosanoid was optimized for maximal signal using flow injection mass spectrometry. Eicosanoids were identified in samples by matching their MRM signal and LC retention time with those of a pure standard. Extraction and ionization efficiencies were determined for the internal standards by comparing the ion intensity of the samples with those of the extraction controls. The range of efficiency for a typical experiment was between 20 and 75%, with an average of around 50%.

Quantitative Eicosanoid Analysis—Quantitative eicosanoid determination was performed by the stable isotope dilution method (21, 22). Deuterated internal standards (2.5 ng) were added to each sample to account for extraction efficiency and mass spectrometry ion suppression. To calculate the amount of eicosanoid in a sample, the ratio of the natural eicosanoid peak area to the deuterated eicosanoid peak area (termed "eicosanoid ratio") was determined for each sample. The eicosanoid ratio, proportional to ng of eicosanoid, was converted using the standard curve, 2.5 ng of each internal (deuterated) eicosanoid standard mixed with the following amounts of natural eicosanoid (nondeuterated) primary standard: 0.1, 0.3, 1, 3, 10, 30, and 100 ng. The hepoxilin standards that are commercially available from Biomol each contain a mixture of two diasteriomers, which are not distinguishable by this methodology and are identified only as hepoxilin (HX) A_3 and HXB_3, respectively. For PD_1 and Δ15t-PD_1, the isomer 10*S*,17*S*-diHDoHE was used as the quantitative primary standard; for 11β PGE_2, the isomer

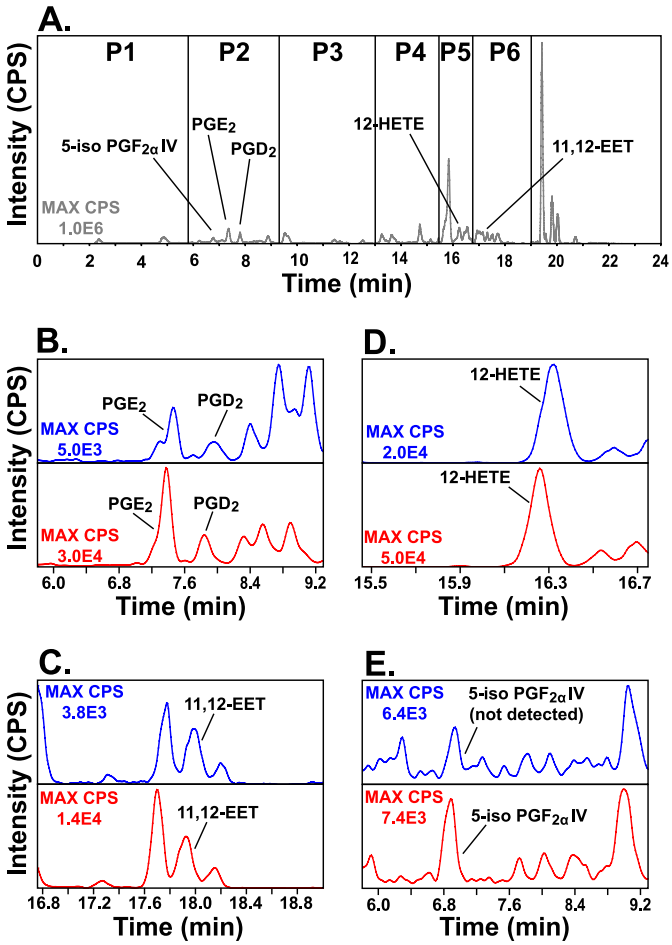

FIGURE 1. **Liquid chromatography-mass spectrometry analysis of ankle joint eicosanoids.** Results from representative chromatograms from C3H/HeJ mouse samples are shown. *A*, total ion chromatogram of a *B. burgdorferi*-infected C3H/HeJ ankle joint. Individual metabolites were measured using MRM transitions, which were divided into six periods (P1–P6). The period following P6 was not used for eicosanoid analysis. *MAX CPS* refers to the maximum total counts/s over the entire 24-min analysis. *B–E*, representative MRM chromatograms of cyclooxygenase (PGE_2 and PGD_2, m/z 351 → 271) (*B*); lipoxygenase (12-HETE, m/z 319 → 179) (*C*); cytochrome P450 (11,12-EET, m/z 319 → 167) (*D*); and non-enzymatic metabolites (5-iso-$PGF_{2\alpha}$ IV, m/z 353 → 115) (*E*). Illustrated are chromatograms of an uninfected (*blue*) and *B. burgdorferi*-infected (*red*) mouse joint, where *MAX CPS* refers to the maximum counts/s of the MRM transition in that period.

PGE_2 was used. Performing linear regression using $Y = mX$, where (Y = eicosanoid ratio, X = ng of eicosanoid, m = slope), the eicosanoid ratio was multiplied by $(1/m)$ to determine the ng eicosanoid in a sample. The deuterated internal standards contained a small but detectable level of natural, undeuterated eicosanoid; to account for this, extraction controls were performed in quadruplicate and the ng of eicosanoid subtracted from each sample. The final values were normalized to the original weight of the tissue and expressed as ng of eicosanoid/mg of tibiotarsal tissue.

Heat Maps—In addition to quantitative analysis, data were expressed as a heat map to identify relative increases and decreases in metabolites over time. Similar to the quantitative analysis, the extraction eicosanoid ratio was subtracted from the sample ratio and normalized to the original weight of the tissue; this value was then normalized to the corresponding value at day 0. The $(1/m)$ value determined from the quantitative curve cancels out of relative fold calculations. One advantage to eliminating $(1/m)$ is that, for eicosanoids with a limited availability, analysis can be performed in the absence of full quantitation.

Statistics—Results are expressed as the means ± S.E. Comparisons were made using one-way analysis of variance followed by a multiple comparison procedure, or t test, and p values ≤ 0.05 were considered significant.

RESULTS

Murine Model of Lyme Arthritis—Upon infection with *B. burgdorferi,* arthritis-susceptible C3H/HeJ (C3H) mice developed a severe inflammatory response as measured by arthritis severity scores, which peaked at 2 weeks post-infection and then spontaneously resolved. Resistant DBA/2J (DBA) mice developed only a very mild inflammation (Fig. 2*A*). Bacterial loads in the joint tended to mirror the course of pathology (Fig. 2*B*), peaking just before the arthritic response. However, inoculum size does not affect susceptibility or resistance to arthritis development in most mouse strains (23). The difference in histopathology was most evident at the peak of arthritis, the development of which is dependent upon neutrophil recruitment into the infected joint (Fig. 2*C*, day 10) (19), whereas macrophages predominated during the resolution phase (Fig. 2*C*, day 35) (16). Resolution of arthritis is attributed to *B. burgdorferi*-specific IgM- and IgG-mediated (Fig. 2*D*) clearance of bacteria from infected joints (24). Overall, DBA mice demonstrated less cellular infiltration into the joints with almost no differences in the bacterial loads and antibody responses, demonstrating that Lyme arthritis susceptibility is genetically regulated and independent of the numbers of bacteria in the joints (25).

Lipidomic Analysis of Infected Joints—Tibiotarsal (ankle) joints from *B. burgdorferi*-infected C3H and DBA mice were collected at various time points post-infection and analyzed for eicosanoid levels during the progression of arthritis (Fig. 3). The majority of joint mass is bone, making it difficult to extract the low levels of eicosanoids from the surrounding tissue comprised of infiltrating cells, muscle, synovium, intrarticular fluid, and cellular exudate. Joints were kept frozen with liquid nitrogen and then pulverized. The resultant powder was placed in cold 50% ethanol containing an antioxidant mixture to prevent lipid degradation. After 72 h of incubation at −20 °C, samples were clarified by centrifugation and supernatants dried completely under nitrogen gas. Repeated analysis found dramatically decreased eicosanoid levels with −20 °C incubation times less than 72 h and little to no increase in lipid concentrations with incubation times greater than 72 h. Samples were reconstituted with 10% methanol containing 21 deuterated internal standards representative of products from all major eicosanoid biosynthetic pathways. Subsequently, the samples were purified by solid phase extraction and stored in methanol for analysis (21, 22).

Eicosanoids were analyzed using liquid chromatography coupled with tandem mass spectrometry. Upon injection, eicosanoids were eluted using a 25-min reverse phase liquid chromatography gradient capable of separating the majority of known eicosanoids. Following LC separation, each eicosanoid

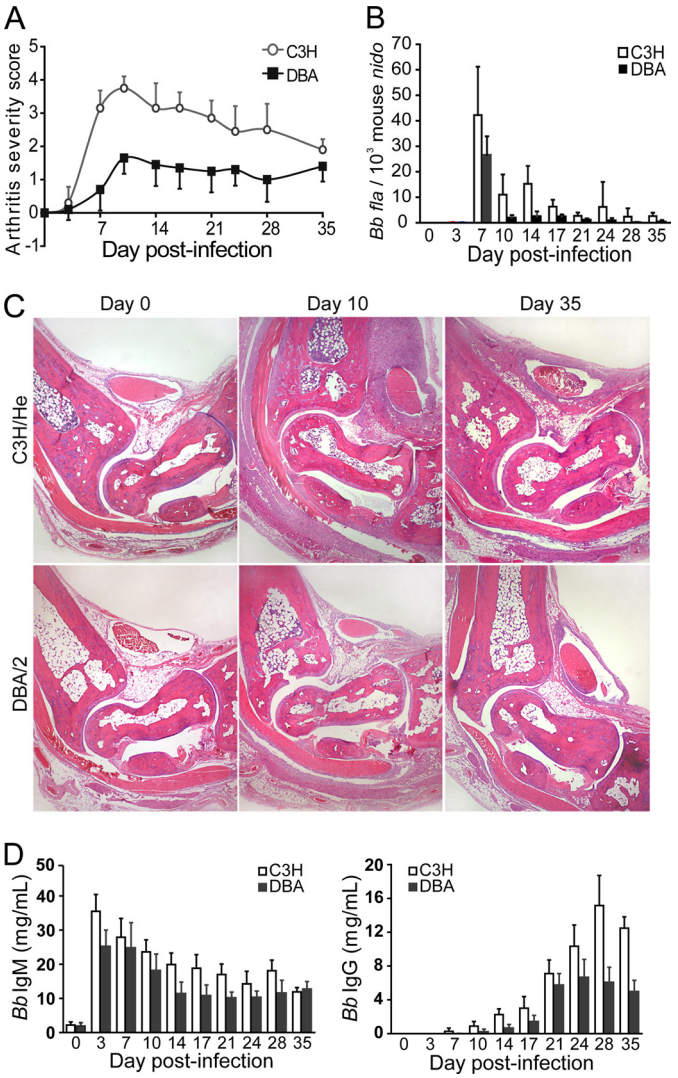

FIGURE 2. **Differential development of experimental Lyme disease in resistant DBA and susceptible C3H mice.** C3H/HeJ and DBA/2J mice were infected with 1×10^5 *B. burgdorferi* and sacrificed at the indicated time points from day 0 through day 35 post-infection. *A*, arthritis severity scores were determined by histological examination of hematoxylin and eosin-stained sections of the tibiotarsal joints. *B*, *Borrelia* loads in the knee joint as determined by real-time PCR. *C*, representative sections of ankle joints from C3H (*upper panels*) and DBA (*lower panels*) mice before infection (day 0) and during the peak and resolution phases of the inflammatory response to *Borrelia* infection (day 10 and day 35 post-infection, respectively; ×100 magnification). *D*, production of *B. burgdorferi*-specific IgM and IgG throughout infection. All results are expressed as the mean ± S.E. and are representative of two experiments. ($n = 5$ mice/time point/group).

was selected for identification using MRM, whereby the mass spectrometer identified a given molecule by its parent mass and a characteristic fragment ion generated in the second quadrupole. In combination with the LC retention time, this technique can distinguish large numbers of eicosanoids in a single analysis (Fig. 1, supplemental Table 1). The mass spectrometer duty cycle limits the number of MRM transitions that can effectively be run simultaneously, and thus they were separated into six different temporal analysis periods. The average detection limit using this method was 10.5 pg, with more than 80% of the metabolites in this method detectable at this level. Eicosanoids were measured using the stable isotope dilution method, which assesses each metabolite as the ratio of signal from the eicosanoid to that of the isotopically distinguishable internal standard (22). Using stable isotope dilution quantitation helps diminish the potential error due to extraction, purification, and matrix effects that undoubtedly arise from tissue samples.

In total, 49 or 47 unique molecular species were detected in joints from C3H or DBA mice, respectively, including metabolites derived from cyclooxygenase, lipoxygenase, cytochrome P450, and non-enzymatic and degradative pathways. In contrast, only 41 were detected in sham-infected joints. Significant temporal changes in the COX, LOX, and CYP pathways were identified in both C3H and DBA mice during the course of infection (Fig. 3). In C3H mice, the majority of these eicosanoids were generally elevated between days 3 and 17 post-infection. Arthritis-resistant DBA mice generated a similar but muted metabolic profile, concentrated temporally in days 7 and 10. Non-enzymatically generated isoprostane eicosanoids increased dramatically in C3H mice, indicating massive changes in oxidative stress, which correlated with the severity of arthritis in this strain. Sham-infected C3H mice showed no significant changes in eicosanoid production in the ankle joint (supplemental Fig. S1). Selected metabolites from each of the eicosanoid classes are described herein, and their proposed contribution to the inflammatory response is suggested and subsequently used to develop a model of eicosanoid dynamics during the induction and resolution of inflammation in response to *B. burgdorferi* infection. The complete quantitative data set has been made available (supplemental Tables 2–4).

COX and CYP Metabolites—Previous studies examining models of rheumatoid arthritis and other models of autoimmunity have defined PGE_2 and PGD_2 as classic pro-inflammatory COX products that induce and regulate inflammatory responses, as well as some aspects of adaptive immunity, such as T cell activation and cytokine expression (26, 27). During experimental Lyme arthritis, PGE_2 and PGD_2 levels increased in C3H mice beginning at day 3 and returned to basal levels by day 17 (Fig. 4, *A* and *B*), preceding both bacterial clearance from the joint and the production of *B. burgdorferi*-specific IgG antibodies. Arthritis-resistant DBA mice produced high levels of PGE_2 from days 7 through 10; however, PGD_2 was not significantly increased during infection. PGD_2 can be hydrolyzed to 15d PGJ_2, which purportedly exerts anti-inflammatory effects by inhibiting NF-κB and activating peroxisome proliferator-activated receptor γ (28, 29). However, work demonstrating this effect was performed primarily *in vitro*, and thus its role *in vivo* remains controversial (30). Joints from both strains contained significant levels of 15-d PGJ_2 at d7, as well as at d3 in C3H animals (Fig. 4*C*). PGE_2 is cleared from the extracellular milieu by enzymatic oxidation to form the less bioactive metabolite 15k-PGE_2. Production of this metabolite followed a pattern similar to that of its precursor and was detected at high levels from d3 through d21 post-infection in both DBA and C3H mice (Fig. 4*D*). These data suggest that PGE_2 and PGD_2 may promote the onset of the inflammatory response, possibly by inducing the production of neutrophil-chemotactic molecules such as CXCL-1 and CXCL-2, the production of which are responsive to PG levels and which have previously been implicated in the development of Lyme arthritis (19, 31, 32). Additionally, these eicosanoids may affect the adaptive

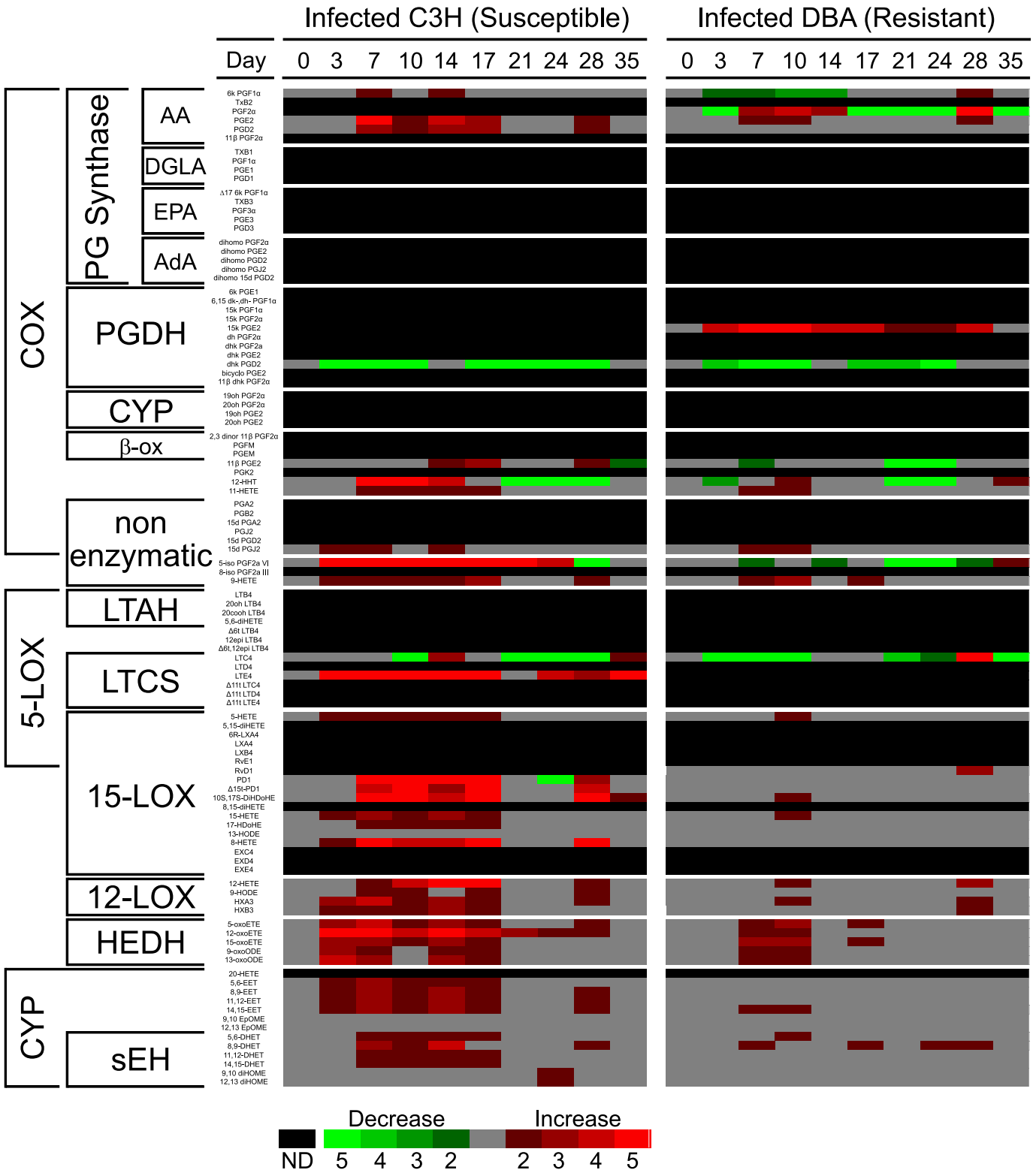

FIGURE 3. **Lipidomic profiling reveals temporal changes in major eicosanoid biosynthetic pathways.** Heat map representing -fold change in the levels of 104 eicosanoid species relative to d0 (uninfected) values for ankle joints of *B. burgdorferi*-infected C3H (arthritis-susceptible) and DBA (arthritis-resistant) mice. Increases in metabolite levels are indicated by *red*, decreases by *green*, and detectable but unchanged levels by *gray*. Metabolites below the limit of detection at d0 (*ND*) are indicated by *black*. $n = 8–10$ mice/time point/group.

immune response by regulating the activation of antigen-presenting cells such as dendritic cells and macrophages (27, 33).

EETs are produced primarily by the CYP2C and CYP2J epoxygenases and modulate inflammation by promoting vasodilatation, angiogenesis, and cellular proliferation (34), and some have been shown to inhibit NF-κB activity *in vitro* (35, 36). Soluble epoxide hydrolase terminates EET signaling by hydrolysis to biologically inactive dihydroxyeicosatrienoic

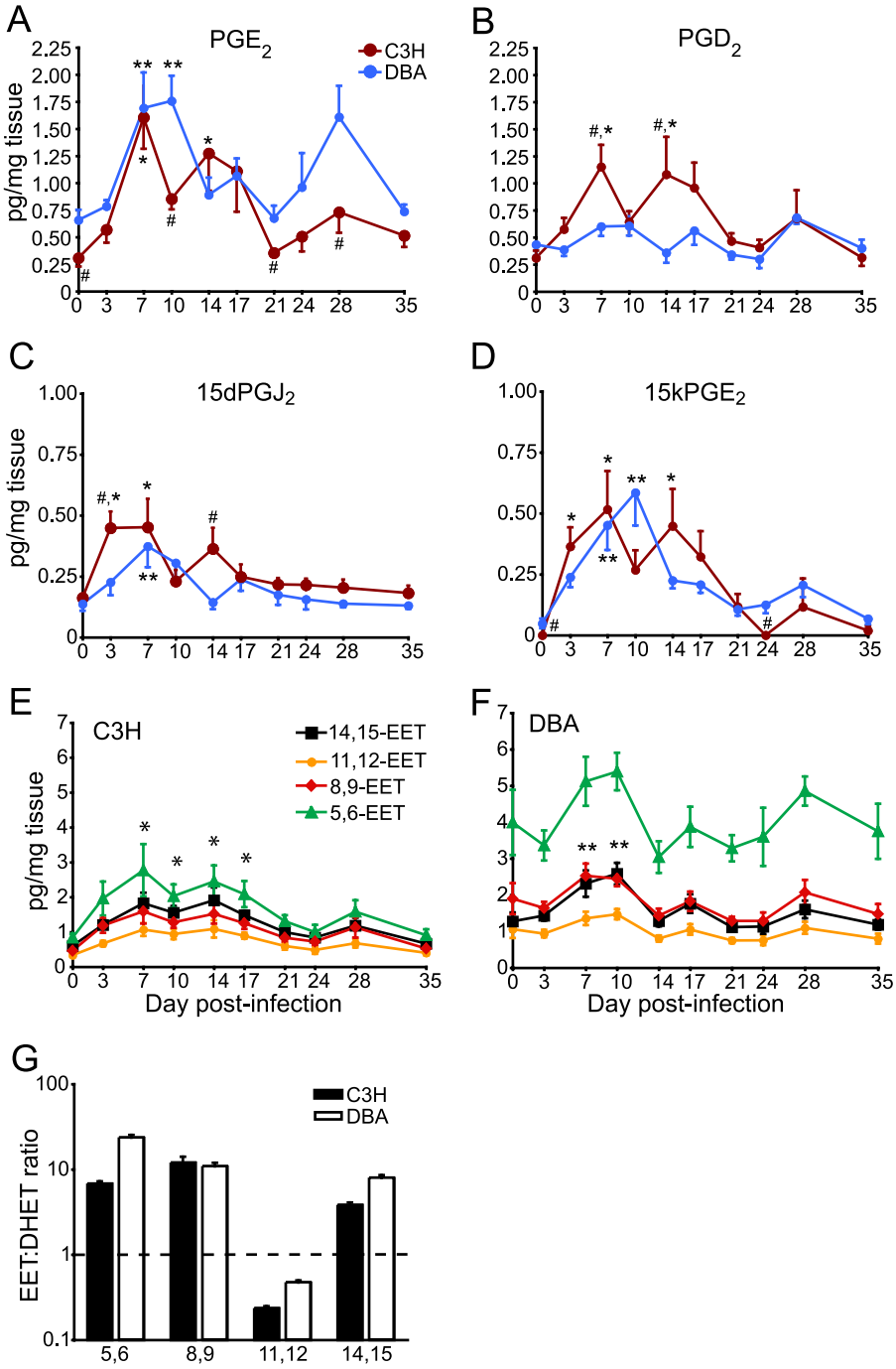

FIGURE 4. **Temporal production of COX and CYP metabolites in C3H and DBA mice during *B. burgdorferi* infection.** *A–D*, time course of PGE_2 and PGD_2 and their metabolites, 15d-PGJ_2 and 15k-PGE_2, in ankle joints of *B. burgdorferi*-infected C3H (*red*) and DBA (*blue*) mice from d0 to d35 post-infection. *, $p < 0.05$, C3H *versus* d0 values; **, $p < 0.05$, DBA *versus* d0 values; #, $p < 0.05$, C3H *versus* DBA at the same time point. *E* and *F*, time course in ankle joints of *B. burgdorferi*-infected C3H (*E*) and DBA (*F*) mice for 5,6-EET (*triangle*), 8,9-EET (*diamond*), 11,12-EET (*circle*), and 14,15-EET (*square*). In the *C3H panel* (*E*), all of the compounds were significantly different from d0 at the indicated time points. In the *DBA panel* (*F*), only 14,15-EET was significantly different from d0 at the indicated time points. *G*, overall ratio of EET:DHET production during *B. burgdorferi* infection. The average (5,6; 8,9; 11,12; or 14,15) EET production across all time points was divided by the average of the respective DHET across all time points to determine the cumulative EET:DHET ratios for C3H (*filled bars*) or DBA (*open bars*) ankle joints. All results are expressed as the mean ± S.E. ($n = 8–10$ mice/time point/group).

acids (DHET) (37). Vascular tone is of interest during the response to infection because vasodilation permits the extravasation of immune cells into the tissue to confront infectious organisms. However, EET or DHET production has not yet been identified in the context of infection. During the course of *B. burgdorferi* infection, C3H mice demonstrated increases in EETs and DHETs from day 7 to day 17 and on day 28 (Fig. 4*E* and supplemental Table 2). EETs also increased in DBA mice at days 7 and 10, returning to basal levels subsequent to bacterial clearance from the joints (Fig. 4*F*). Production levels were similar between C3H and DBA mice for all of the EETs except for 5,6-EET, which was present at much higher levels relative to both C3H 5,6-EET levels and the other three EETs in DBA joints. The ratio of any given EET/DHET pair remained constant through the time of infection in both C3H and DBA mice (supplemental Fig. S2, *A* and *B*), suggesting that soluble epoxide hydrolase activity was unaffected by *B. burgdorferi* infection. However, whereas 5,6-EET, 8,9-EET, and 14,15-EET were 6-, 12-, and 4-fold, respectively, more prevalent than their corresponding DHET, 11,12-EET was 4-fold *less* abundant than 11,12-DHET (Fig. 4*G*). Node *et al.* (35) showed that 11,12-EET specifically prevents leukocyte recruitment by decreasing NF-κB-regulated vascular cell adhesion molecule (VCAM) expression in a model of vascular inflammation, whereas similar effects have been demonstrated with all four EETs using an *ex vivo* model of blood vessel laminar flow (36). It is unlikely that soluble epoxide hydrolase selectively metabolizes 11,12-EET, because the rank order of degradation rate is 14,15-EET > 11,12-EET = 8,9-EET (37, 38). However, any 11,12-EET interacting with NF-κB would be covalently bound and undetected by our assay, leading to the appearance of increased metabolism. This suggests that EETs, specifically 11,12-EET, might play an important role during infection-induced inflammation by counterbalancing pro-inflammatory signals.

Lipoxygenase Metabolites—Mammalian LOX can be classified according to enzymatic activity (5-LOX, 8-LOX, 12-LOX, 15-LOX) or phylogenetic relatedness (4, 39). 5-LOX activity is attributed to a single, highly conserved protein that creates a diverse range of pro- and anti-inflammatory signals. 5-LOX

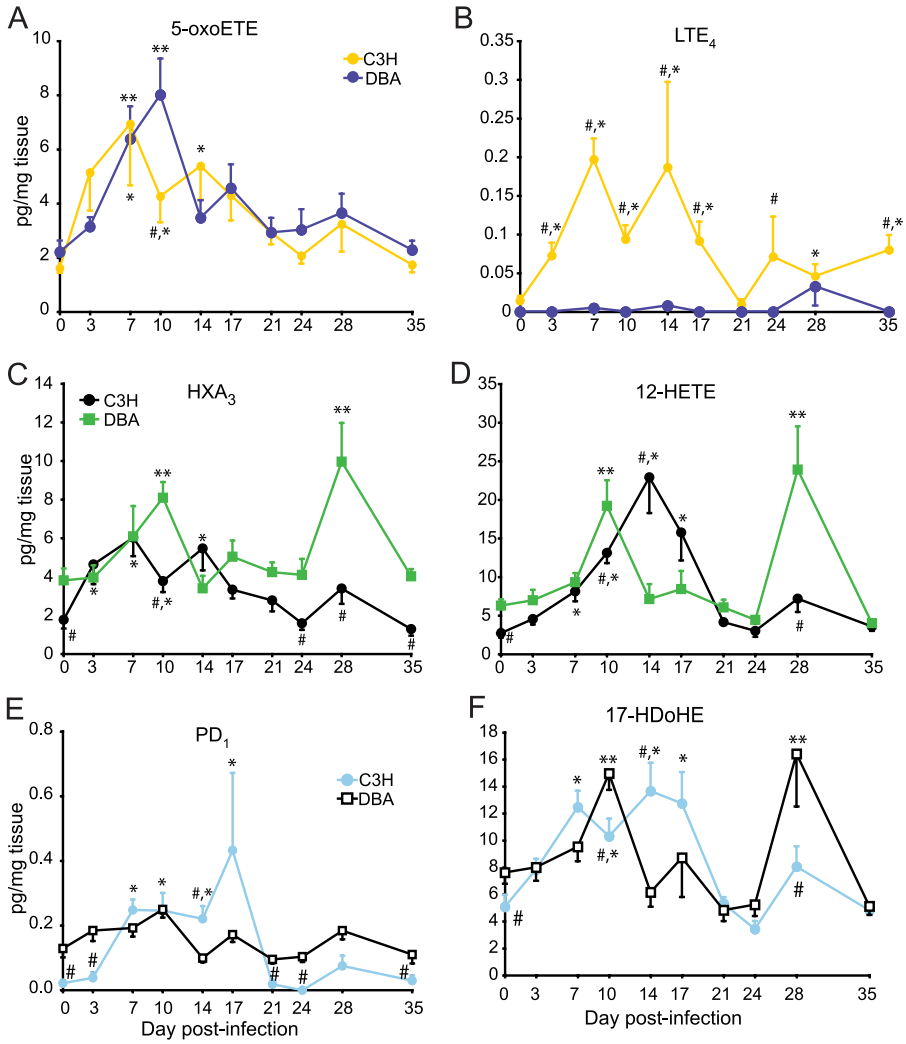

FIGURE 5. **C3H and DBA mice differentially produce LOX and DHA metabolites.** *A* and *B*, time course of 5-LOX products 5-oxoETE and LTE_4, in ankle joints of *B. burgdorferi*-infected C3H (*yellow*) and DBA (*purple*) mice from d0 through d35 post-infection. *C* and *D*, temporal production of 12-LOX metabolites HXA_3 and 12-HETE in ankle joints of C3H (*black*) and DBA (*green*) mice from day 0 through day 35 post-infection. *E* and *F*, temporal production of pro-resolution PD_1 and a stable form of its biosynthetic intermediate, 17-HDoHE, during *B. burgdorferi* infection in ankle joints of C3H (*blue*) and DBA (*black*) mice from day 0 through day 35 post-infection. Results are the mean ± S.E. ($n = 8–10$ mice/time point/group). *, $p < 0.05$, C3H *versus* d0 values; **, $p < 0.05$, DBA *versus* d0 values; #, $p < 0.05$, C3H *versus* DBA at the same time point.

catalyzes the rate-limiting step for the synthesis of leukotrienes, important products and regulators of innate immune cell function and powerful neutrophil chemoattractant signals (40). It also facilitates the formation of 5-HETE from arachidonic acid, which can be further oxidized by neutrophils to 5-oxoETE, which has been shown to be highly chemotactic for eosinophils (41). In *B. burgdorferi*-infected C3H mice, neutrophil influx corresponded to changes in both of these pathways. Similar to the prostaglandins, 5-oxoETE levels increased in C3H mice starting at day 3 and returned to basal levels by day 21 (Fig. 5*A*). DBA mice also demonstrated significantly increased 5-oxoETE levels at d7 and d10 post-infection, which then quickly dropped to near basal levels by d14. The levels of LTE_4 were dramatically affected during the immune response in C3H mice (Fig. 5*B*) and were significantly increased at all but two time points (d21 and d24 post-infection). Remarkably, no cysteinyl leukotrienes were detected at significantly elevated levels in DBA joints. Thus, the production of 5-LOX metabolites corresponded with the intensity of neutrophil recruitment to the site of *B. burgdorferi* infection.

The different murine paralogues of 12-LOX and 15-LOX (12/15-LOX) mediate the formation of 12-hydroperoxyeicosatetraenoic acid, whereupon cellular peroxide levels and sequence-specific protein activities determine its further metabolism. The leukocyte 12/15-LOX protein is highly expressed in murine cells of the monocyte lineage, especially resident macrophages, and its expression correlates with that of a diverse array of chemokines and cytokines (42, 43). In a model of acute sterile inflammation, mice lacking this specific 12/15-LOX gene exhibited increased monocyte/macrophage influx, and these cells expressed a cytokine profile reminiscent of anti-inflammatory cells, including lower levels of macrophage chemoattractant protein-1 (MCP-1; CCL2) and interleukin-17 (43). 12-Hydroperoxyeicosatetraenoic acid can be reduced to 12-HETE, which promotes monocyte chemotaxis *in vitro* by inducing MCP-1 expression (44) and *in vivo* induces monocyte adhesion through epithelial intercellular adhesion molecule (ICAM) up-regulation in a murine model of atherosclerosis (45). Alternatively, 12-hydroperoxyeicosatetraenoic acid can be isomerized to form biologically inert HXB_3 or the biologically active HXA_3, which elicits neutrophil chemotaxis without superoxide production or granule release *in vitro* (46). *In vivo* results are equivocal; administration of HXA_3 inhibits fibrosis and suppresses inflammatory macrophage recruitment in a model of bleomycin-induced lung injury (47); however, HXA_3 is required for the recruitment of neutrophils in some models of mucosal infection (48). *B. burgdorferi* -infected C3H mice produced HXA_3 at significantly increased levels between days 3 and 14, whereas DBA production of HXA_3 in DBA strains spiked at days 10 and 28 post-infection (Fig. 5*C*). Hepoxilin B_3 was detected at lower levels in both strains during the same period (supplemental Tables 2 and 3). 12-HETE levels steadily rose in C3H joints during the induction phase of inflammation, peaking at day 14 and then returning to base-line levels by d21 post-infection (Fig. 5*D*). Similar to HXA_3, 12-HETE peaked at d10 and d28 in DBA mice. Our results for 12-HETE and HXA_3

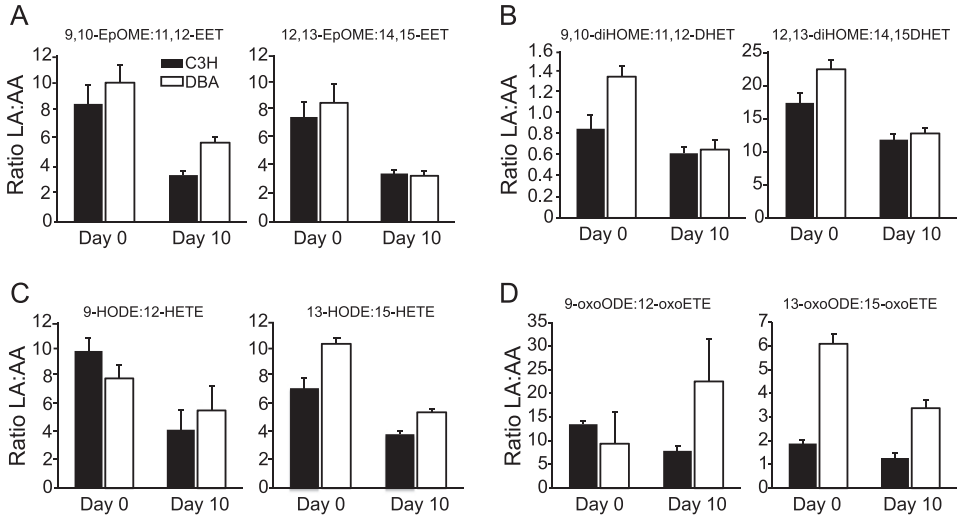

FIGURE 6. **Concentrations of linoleic acid metabolites are severalfold higher than arachidonic acid metabolites in C3H and DBA ankle joints.** *A–D*, ratio of linoleic acid metabolites to their arachidonic acid counterparts at day 0 (basal) and day 10 post-infection with *B. burgdorferi* in both C3H (*filled bars*) and DBA (*open bars*) ankle joints. For each time point, the average concentration of the linoleic acid metabolite was divided by the concentration of the respective arachidonic acid metabolite. Values are expressed as the mean ratio of linoleic acid metabolite (*LA*) *versus* arachidonic acid metabolite (*AA*) ± S.E. (n = 8–10 mice/time point/group).

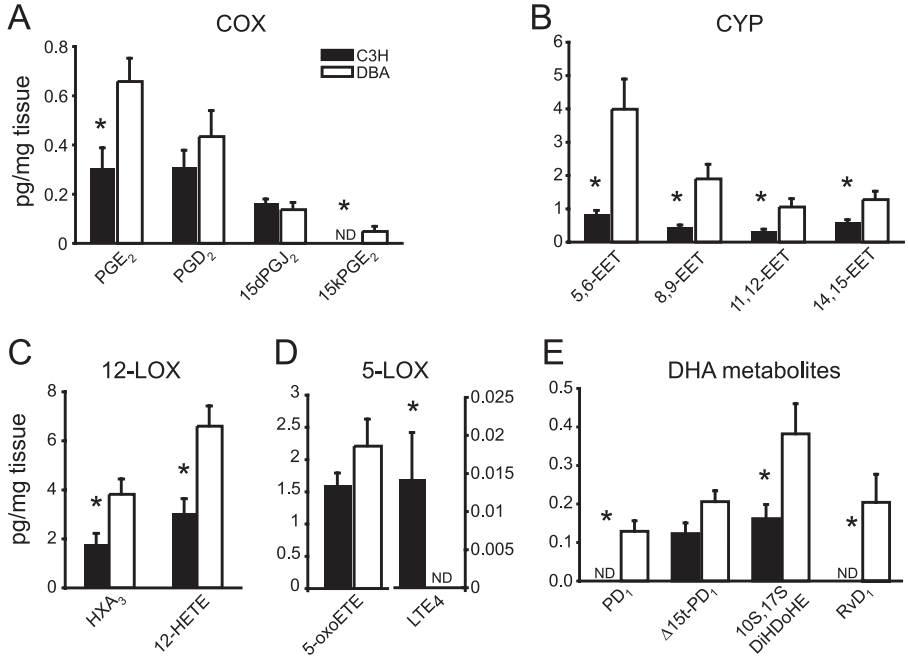

FIGURE 7. **Differential basal production of eicosanoids from all major enzymatic pathways in C3H *versus* DBA ankle joints.** *A–E*, basal production of: *A*, COX products PGE_2, PGD_2, 15d-PGJ_2, and 15k-PGE_2; *B*, CYP products 5,6-EET, 8,9-EET, 11,12-EET, and 14,15-EET; *C*, 12-LOX products HXA_3 and 12-HETE; *D*, 5-LOX products 5-oxoETE and LTE_4; and *E*, DHA metabolites PD_1, Δ15t-PD_1, 10*S*,17*S*-diHDoHE, and RvD_1 in ankle joints from C3H (*filled bars*) and DBA (*open bars*) mice. *ND*, not detected. *, $p < 0.05$, C3H *versus* DBA. All results are expressed as the mean ± S.E. (n = 8–10 mice/time point/group).

rophages, platelets, or endothelial cells (6, 49). Therapeutically administered protectins have anti-inflammatory properties, such as the reduction of neutrophil influx, and pro-resolution properties, including the recruitment of monocytes, the activation of anti-inflammatory macrophages, and the phagocytosis of cellular and microbial debris (6, 50). Although LXA_4 concentrations have been determined in serum by enzyme-linked immunosorbent assay in a model of parasite infection (51), lipoxins have not previously been measured by LC-MS/MS from tissue during infection. Additionally, neither Rv nor PD have been measured in tissue following infection. Protectins were identified in *B. burgdorferi*-infected joints from both mouse strains. PD_1 increased 5–10-fold from days 7 to 17 in C3H joints, whereas DBA mice did not demonstrate a significant increase in PD_1 levels during *B. burgdorferi* infection (Fig. 5*E*). The less biologically active protectin isomers, Δ15t-PD_1 and 10*S*,17*S*-diHDoHE, were also generated at higher concentrations in C3H than in DBA joints in response to infection (supplemental Fig. S3, *A* and *B*). PD_1 was 4-fold less abundant than 10*S*,17*S*-diHDoHE; however, it has been shown to block neutrophil influx with greater potency *in vivo*, which suggests that PD_1 may have a physiologically important role in controlling the response to *B. burgdorferi* infection (52). Additionally, at various time points post-infection, C3H mice demonstrated significantly higher levels of 17-HDoHE, a stable form of the Rv and PD biosynthetic intermediate 17-HpDoHE (Fig. 5*F*) (53). At d14, 17-HDoHE was produced at >1-fold levels in C3H joints *versus* DBA; however, this situation was reversed at d28, when DBA mice produced significantly greater levels than C3H mice. Collectively, these data suggest that, although they posses the ability to produce pro-resolution and anti-inflammatory molecules, C3H mice may have a functional defect in the metabolism of precursor molecules and a higher threshold for the response to this group of metabolites, resulting in less effective control of the inflammatory response to infection.

imply that during a sustained, long term model of an inflammatory response, such as infection, these molecules may perform dual roles by recruiting cells to clear bacteria from the site of infection and also counterbalancing pro-inflammatory signals produced at the same time.

LX, Rv, and PD comprise a class of lipid mediators produced by the action of a transcellular enzyme cascade of LOXs and epoxygenases that are differentially expressed between heterogeneous combinations of neutrophils, mac-

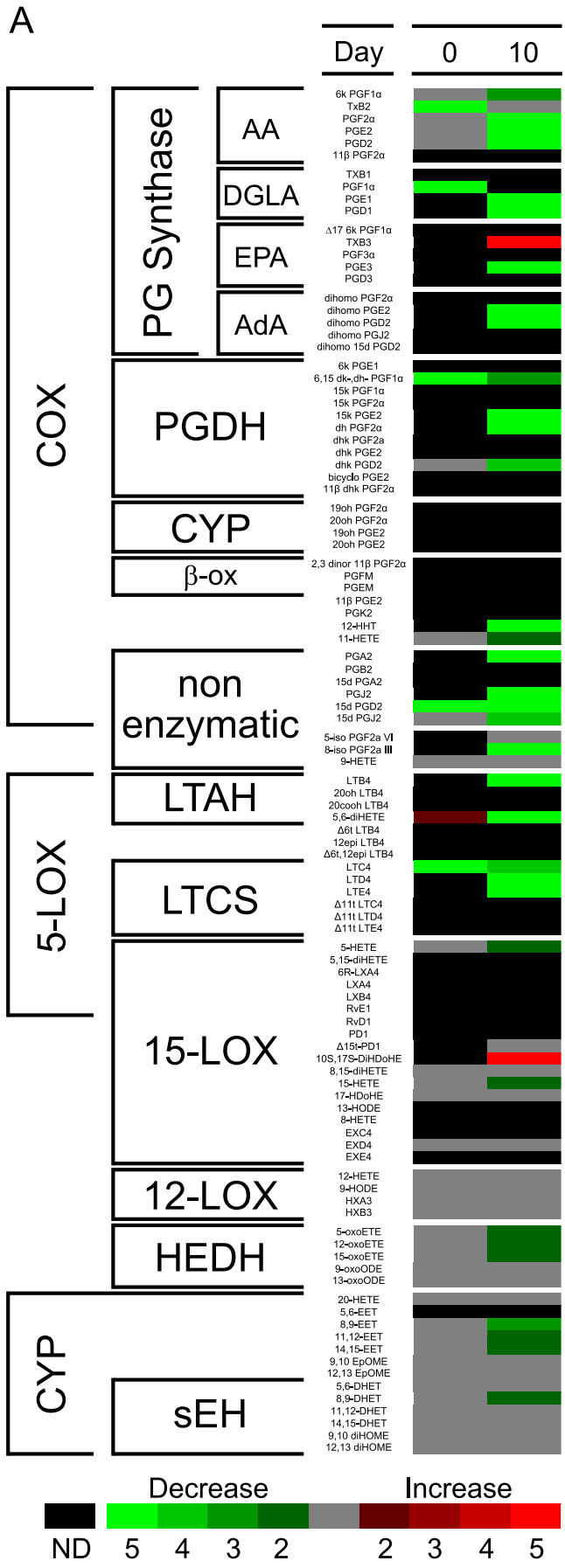
A
Day
0
10
COX
PG Synthase
AA
DGLA
EPA
AdA
PGDH
CYP
β-ox
non enzymatic
5-LOX
LTAH
LTCS
15-LOX
12-LOX
HEDH
CYP
sEH
6k PGF1α
TxB2
PGF2α
PGE2
PGD2
11β PGF2α
TXB1
PGF1α
PGE1
PGD1
Δ17 6k PGF1α
TXB3
PGF3α
PGE3
PGD3
dihomo PGF2α
dihomo PGE2
dihomo PGD2
dihomo PGJ2
dihomo 15d PGD2
6k PGE1
6,15 dk-dh-PGF1α
15k PGF1α
15k PGF2α
15k PGE2
dh PGF2α
dhk PGF2α
dhk PGE2
dhk PGD2
bicyclo PGE2
11β dhk PGF2α
19oh PGF2α
20oh PGF2α
19oh PGE2
20oh PGE2
2,3 dinor 11β PGF2α
PGFM
PGEM
11β PGE2
PGK2
12-HHT
11-HETE
PGA2
PGB2
15d PGA2
PGJ2
15d PGD2
15d PGJ2
5-iso PGF2a VI
8-iso PGF2a III
9-HETE
LTB4
20oh LTB4
20cooh LTB4
5,6-diHETE
Δ6t LTB4
12epi LTB4
Δ6t,12epi LTB4
LTC4
LTD4
LTE4
Δ11t LTC4
Δ11t LTD4
Δ11t LTE4
5-HETE
5,15-diHETE
6R-LXA4
LXA4
LXB4
RvE1
RvD1
PD1
Δ15t-PD1
10S,17S-DiHDoHE
8,15-diHETE
15-HETE
17-HDoHE
13-HODE
8-HETE
EXC4
EXD4
EXE4
12-HETE
9-HODE
HXA3
HXB3
5-oxoETE
12-oxoETE
15-oxoETE
9-oxoODE
13-oxoODE
20-HETE
5,6-EET
8,9-EET
11,12-EET
14,15-EET
9,10 EpOME
12,13 EpOME
5,6-DHET
8,9-DHET
11,12-DHET
14,15-DHET
9,10 diHOME
12,13 diHOME
Decrease
Increase
ND 5 4 3 2 2 3 4 5
B
COX
WT
KO
pg/mg tissue
PGE2
PGD2
15kPGE2
15dPGJ2
CYP
11,12EET
14,15 EET
11,12 DHET
14,15 DHET
12/15-LOX
HXA3
12-HETE
10S,17S DiHDoHE
5-LOX
5-HETE
5-oxoETE
LTC4
LTE4

Linoleic Acid Metabolites—Linoleic acid is an 18-carbon polyunsaturated fatty acid containing only two double bonds, limiting its utility as a substrate for eicosanoid biosynthetic enzymes in comparison with arachidonic acid. CYP epoxygenation of linoleic acid forms 9,10- and 12,13-epoxyoctadecamonoenoic acid, commonly classified as leukotoxins, which are generated from activated neutrophils and macrophages and can induce cell death (54). The toxic effects of these metabolites are thought to be mediated by their conversion into the corresponding diols, 9,10- and 12,13-diHOME, by soluble epoxide hydrolase (55). Analogous to arachidonic acid-derived HETEs, both CYP and LOX can hydroxylate linoleic acid to form HODEs, which can subsequently be oxidized to form oxooctadecadienoic acids (oxoODEs). These metabolites have been shown to be potent activators of peroxisome proliferator-activated receptor γ (56).

In contrast to arachidonic acid, the CYP metabolites of linoleic acid metabolites did not demonstrate dramatic temporal changes in response to *B. burgdorferi* infection (supplemental Tables 2 and 3). Whereas 12-HETE levels steadily rose over the first 14 days of infection in C3H mice, high levels of 9-HODE and 13-HODE were produced throughout infection. In general, linoleic acid metabolites demonstrated more variability between samples than those from arachidonic acid, making it difficult to discern a temporal pattern for their production. Interestingly, in both mouse strains the amount of a given linoleic acid metabolite was typically 4–20 times higher than its corresponding arachidonic acid metabolite (Fig. 6). This may be due to the comparatively higher amounts of linoleic acid found in mammalian tissues (57). However, given their potentially important bioactivity, these data indicate that this class of metabolites warrants consideration and further investigation.

Arthritis-susceptible Mice Have an Altered Basal Eicosanoid Profile—Although the peak levels of many COX, LOX, and CYP metabolites were comparable between the two strains, several eicosanoids in DBA joints exhibited basal production levels above those seen in C3H mice. In light of the fact that many of these lipids are considered "pro-inflammatory," it seemed counterintuitive for base-line levels of these molecules to be higher in the Lyme arthritis-resistant mice, which exhibited a milder inflammatory response as compared with the severe arthritis demonstrated in C3H mice. In some cases, this necessitated a severalfold increase in production above that seen in DBA joints in order to reach a similar tissue lipid concentration. For instance, pro-inflammatory PGE_2 was present in C3H joints at 50% of the basal levels found in the resistant DBA strain (Fig. 7*A*). Similarly, the anti-inflammatory EETs were all produced at significantly lower basal levels in C3H *versus* DBA joints (Fig. 7*B*). Both pro-inflammatory HXA_3 and anti-inflammatory 12-HETE basal levels were 1–2-fold higher in DBA than in C3H mice (Fig. 7*C*). Taken alone, decreased levels of these lipids suggest there should be less inflammation in C3H mice. However, C3H mice also demonstrated high basal levels of LTE_4 (Fig. 7*D*) and little to no basal production of the pro-resolving protectins and RvD_1 (Fig. 7*E*). Although RvD_1 did not change significantly during the course of infection (supplemental Tables 2 and 3), differences in basal pro-resolution metabolite levels could alter the inflammatory tone, priming C3H mice toward a stronger inflammatory response. These surprising data suggest that the lipids produced by the microenvironment at homeostasis may be just as important as lipid production throughout the response to infection. Overall, the basal levels of several eicosanoids observed in DBA mice were higher than in the C3H mice, suggesting a mechanism for the more controlled response to *B. burgdorferi* infection in the DBA strain.

Lipid Metabolic Consequences of COX-2 Deficiency—The above findings illustrate the complexity of the inflammatory response to infection and suggest the potential importance of products from all of the major eicosanoid biosynthetic pathways. To demonstrate the applicability of this approach to the investigation of disease pathogenesis, we utilized this lipidomic protocol to determine eicosanoid levels in the context of COX-2 deficiency. We choose to focus on COX-2 for several reasons. In the clinical setting, patients diagnosed with rheumatoid or Lyme arthritis are typically treated with nonsteroidal anti-inflammatory drugs (NSAIDs) or COX-2-selective inhibitors such as celecoxib (Celebrex™, Pfizer) (15). Numerous studies in animal models of rheumatoid arthritis have illustrated the importance of the COX-2 enzyme in autoimmune arthritis development (58, 59). However, very little is known about the role of eicosanoids in infectious arthritides. Previously we described the development of Lyme arthritis in C3H and DBA mice lacking COX-2 activity (11). Although COX-2 deficiency resulted in attenuated ankle swelling and lower PGE_2 concentrations in the joint, the development of arthritis pathology was unaltered. Importantly, however, mice lacking COX-2 failed to resolve their inflammatory response and demonstrated prolonged arthritis pathology, as characterized by sustained neutrophil influx into the joints. These data were contrary to results in models of autoimmune arthritis, in which a lack of COX-2 activity prevented or ameliorated arthritis (58, 59). These data hinted at the complexity of eicosanoid involvement in regulating the immune response and illustrated the need for in-depth lipidomic analysis.

COX-$2^{-/-}$ and wild-type (WT) littermate controls were infected with *B. burgdorferi*, and lipidomic analysis was performed on ankle joints at d0 and d10 post-infection. This phase of the inflammatory response was chosen because basal levels and early events during infection appear to be the key to orchestrating the subsequent immune response and the outcome of arthritis pathology (11). Global eicosanoid profiles from WT and COX-$2^{-/-}$ C3H mice identified a number of off-target changes (Fig. 8*A* and supplemental Table 5). As expected, PGE_2 and PGD_2 levels were significantly reduced in COX-2 knock-

FIGURE 8. **COX-$2^{-/-}$ mice exhibit decreased levels of 5-LOX products.** *A*, heat map representing -fold change in the levels of 104 eicosanoid species in C3H COX-$2^{-/-}$ mice at d0 or d10 relative to values for WT control animals. Increases in metabolite levels are indicated by *red*, decreases by *green*, and detectable but unchanged levels by *gray*. Metabolites below the limit of detection at d0 (*ND*) are indicated by *black*. *B*, quantitative differences between WT (*filled circle*) and COX-$2^{-/-}$ (*open circle*) mice in the levels of products from the COX, CYP, 12/15-LOX, and 5-LOX pathways. Each symbol represents an individual animal. *Bars* represent the median of the values for each group ($n = 4$ mice/group). *, $p < 0.05$, COX-$2^{-/-}$ *versus* WT controls. Results are representative of two experiments performed.

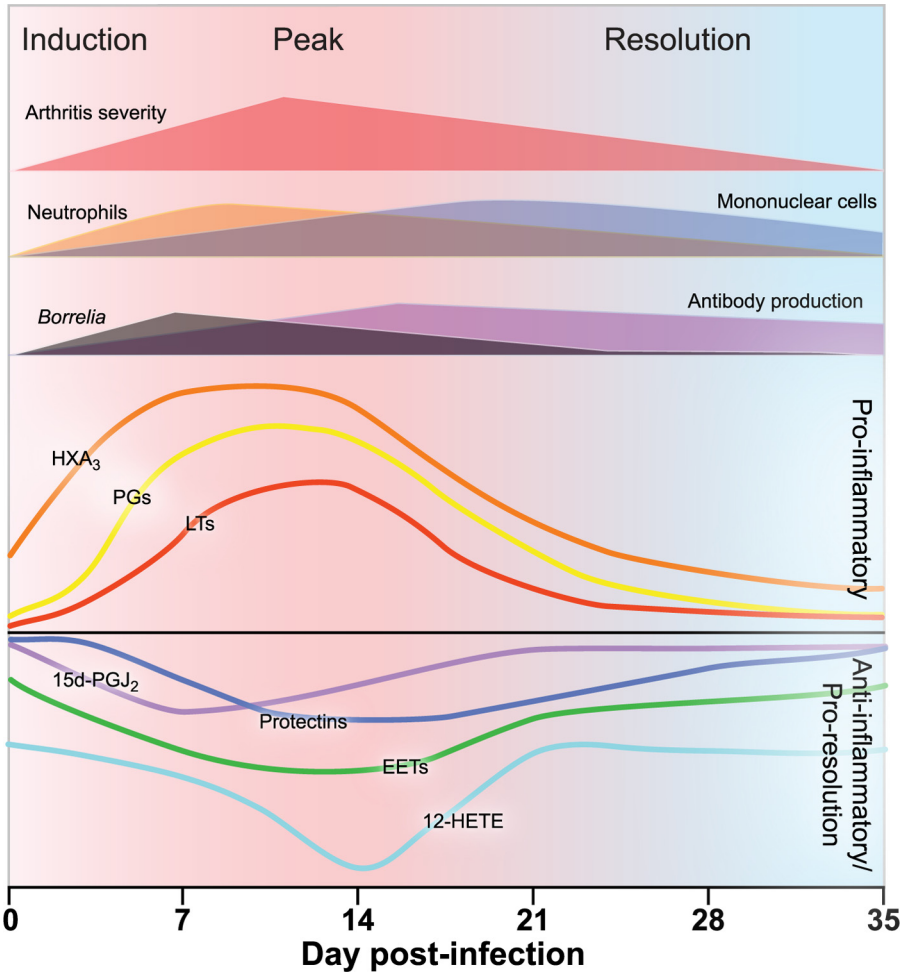

FIGURE 9. **Lipid mediators regulate all phases of *B. burgdorferi* infection.** Pro-inflammatory COX metabolites PGE_2 and PGD_2 are produced early to initiate various aspects of the innate and acquired immune response, whereas 15d-PGJ_2 is produced as an anti-inflammatory counterbalance. 12-LO-derived HXA_3 participates in neutrophil recruitment as 12-HETE modulates monocyte recruitment preceding antibody-mediated *Borrelia* clearance from the joints. DHA-derived protectins collaborate in the control and subsequent resolution of inflammation via the regulation of both leukocyte recruitment and macrophage phagocytosis of apoptotic cells. Throughout infection, EETs control both vascular permeability and the recruitment of mononuclear cells. Decreased production of these and other lipid mediators is indicative of the successful resolution of the inflammatory response and the return to homeostasis.

out mice; likewise, the amounts of the corresponding breakdown metabolites were also decreased (Fig. 8*B*). The loss of COX activity had no significant effect on the CYP-derived EETs or the 12-LOX metabolites HXA_3 and 12-HETE. Surprisingly, elimination of COX-2 activity resulted in a concomitant drop in pro-inflammatory 5-LOX products LTC_4, LTE_4, and 5-HETE. Although at this early time point there was an equal level of infiltrating neutrophils, a key cellular source of LTs, between WT and COX-$2^{-/-}$ the levels of 5-LOX activity dropped dramatically in the tibiotarsal joints of the COX-$2^{-/-}$ mice. Thus, during the response to *B. burgdorferi* infection, arachidonic acid shunting into other eicosanoid pathways may not play a dominant role, in direct contrast to results found with *ex vivo* cell culture systems (60) or *in vivo* molecular stimuli such as bacterial lipopolysaccharide (61). For these reasons, the investigation of inflammatory signaling in infectious disease models, such as experimental Lyme arthritis, coupled with lipidomic analysis may redefine the role that different eicosanoid cascades play on a systemic level during an immune response.

DISCUSSION

Although steps have been taken to increase the number of eicosanoids included in lipidomic-style screens, full scale lipidome analyses have been lacking. Previous attempts at eicosanoid lipidomics have focused on singular pathways or phases of the inflammatory response (10, 14, 62). Although studies of this type increase our knowledge of the inherent potential of certain molecules, they provide an incomplete picture and give the impression that some lipids function in isolation. In reality, they are likely governed by up-stream mediators and, in turn, regulate other metabolites to produce the overall outcome of the inflammatory and immune responses.

Herein we have described a protocol for lipidomic analysis of nearly the entire known eicosanoid lipidome and applied this method to the investigation of infection with a clinically relevant pathogen, *B. burgdorferi*. By initially utilizing two mouse strains with differential susceptibility to the development of Lyme arthritis, analysis of the inflammatory response found production of not only "the usual suspects," such as PGE_2 and PGD_2, but also discovered the production of eicosanoids not previously described during a normal immune response, including CYP and 12-LOX products 11,12-EET and PD_1, respectively. Lipidomic characterization of Lyme arthritis-resistant and -susceptible strains also revealed several unexpected findings. The high basal production of many pro- and anti-inflammatory metabolites in DBA relative to C3H joints implied that the initial setting in which an inflammatory response takes place may be crucial for the eventual disease outcome. Additional analysis found that, although C3H joints contained lower levels of some anti-inflammatory and pro-resolution molecules, they were able to produce high concentrations of precursor molecules, indicating a defect not in the initiation of this particular metabolic cascade but in its completion and intensity.

Analysis of joints from Lyme arthritis-susceptible COX-$2^{-/-}$ animals at early time points post-infection dramatically demonstrated the consequences of perturbing eicosanoid biosynthetic pathways. Previously, inhibition of COX enzymes was expected, at most, to increase production of LOX metabolites due to the possibility of substrate shunting. It is therefore of

great interest that our lipidomic analysis revealed significant decreases in not only COX but 5-LOX products, an effect not previously described in response to the perturbation of the COX-2 pathway.

Based upon our lipidomic analysis of Lyme arthritis-resistant and -susceptible wild-type strains and subsequent analysis of arthritis-susceptible COX-$2^{-/-}$ mice, and using *in vitro* and *in vivo* knowledge of eicosanoid function, we propose the following model to describe the progression of Lyme arthritis (Fig. 9). Early during infection, prostaglandins, leukotrienes, and HXA_3 may cooperate to induce the release of additional pro-inflammatory factors, facilitating the recruitment of neutrophils into the joint and the generation of antibodies to combat *B. burgdorferi* infection. Concomitantly, 15d PGJ_2 and EETs would counterbalance this response by activating peroxisome proliferator-activated receptor γ and inactivating NF-κB, and these are aided later by DHA-derived, pro-resolution protectins. Corresponding to the peak bacterial levels, 12-HETE production peaks, possibly inducing the recruitment of anti-inflammatory macrophages. Once bacteria and neutrophils have been cleared from the site of infection, many of these molecules slowly return to basal levels, indicating a return to homeostasis. Results utilizing COX-$2^{-/-}$ mice further suggested that, although COX metabolites are produced early during infection, COX, and perhaps LOX, products may also be necessary for the subsequent induction of resolution. Undoubtedly, future studies will refine this model; however, it serves as an excellent starting point for probing the complex manner in which eicosanoids collaborate to coordinate an inflammatory immune response.

Susceptibility or resistance to experimental Lyme arthritis does not necessarily translate to susceptibility in other disease models. Interestingly, DBA/2 mice are more susceptible to the development of atherosclerosis and *Pseudomonas aeruginosa*-induced lung injury than are C3H/He mice (63, 64). Tissue-specific cytokine profiles have identified a few differences in protein production; however, lipidomic analysis may reveal tissue-to-tissue differences in the production of eicosanoids that regulate cytokines and chemokines. Just as vascular permeability in the joint differs from that in the skin (65), eicosanoid production likely varies as well. Thus, it will be of interest in the future to investigate basal and induced lipid production in different tissues to determine susceptibility to tissue-specific diseases.

A comprehensive eicosanoid analysis as described herein has a number of attractive clinical applications. In the case of Lyme arthritis, the interruption of specific eicosanoid signals significantly affected the immune response by modulating the recruitment of leukocytes to the infected tissue and their activation. Although interrupting COX signaling reduced one of the cardinal signs of inflammation, swelling, it did not prevent the development of arthritis and had the unintended consequence of impeding resolution by creating global changes in the eicosanoid profile. Studying eicosanoid signaling as a complete system can identify such unforeseen molecular changes. The robustness of this technique lends potential for its easy application beyond the scope of Lyme arthritis to other tissues and diseases. In addition to investigating the mechanisms behind a given disease pathology, this technology could easily be translated into a diagnostic tool for assessing individual patients. The identification of differential eicosanoid production among individual tissue types may open the gate for the development of more disease-specific tissue-targeted therapies and would facilitate the progress of individualized medicine, resulting in more effective treatments with a lower incidence of side effects. Already, genetic screening and microarray technology have philosophically influenced our clinical understanding and treatment of disease (66). A lipidomic platform on a par with this technology has the potential to make an equally profound and complimentary impact. The power of the comprehensive eicosanoid metabolomic analysis described herein lies in its capacity to investigate a naturally progressing inflammation and its potential to translate to clinical diagnosis and treatment of disease.

Acknowledgments—We thank Dr. Richard Harkewicz and Daren L. Stephens for discussions regarding mass spectrometry, Drs. Miguel A. Gijón and David M. Lee for suggestions regarding tissue eicosanoid extraction, and Drs. Darren S. Dumlao and Linda A. Landon for assistance in preparing the manuscript. Protectin D_1, Δ15t-Protectin D_1, Resolvin D_1, and Lipoxin B_4 were kind gifts from Prof. Charles N. Serhan (Harvard University).

REFERENCES

1. Dennis, E. A. (2009) *Proc. Natl. Acad. Sci. U.S.A.* **106,** 2089–2090
2. Schmelzer, K., Fahy, E., Subramaniam, S., and Dennis, E. A. (2007) *Methods Enzymol.* **432,** 171–183
3. Fahy, E., Subramaniam, S., Brown, H. A., Glass, C. K., Merrill, A. H., Jr., Murphy, R. C., Raetz, C. R., Russell, D. W., Seyama, Y., Shaw, W., Shimizu, T., Spener, F., van Meer, G., VanNieuwenhze, M. S., White, S. H., Witztum, J. L., and Dennis, E. A. (2005) *J. Lipid Res.* **46,** 839–861
4. Buczynski, M. W., Dumlao, D. S., and Dennis, E. A. (2009) *J. Lipid Res.* **50,** 1015–1038
5. Funk, C. D. (2001) *Science* **294,** 1871–1875
6. Serhan, C. N., Chiang, N., and Van Dyke, T. E. (2008) *Nat. Rev. Immunol.* **8,** 349–361
7. Roman, R. J. (2002) *Physiol. Rev.* **82,** 131–185
8. Bannenberg, G. L., Chiang, N., Ariel, A., Arita, M., Tjonahen, E., Gotlinger, K. H., Hong, S., and Serhan, C. N. (2005) *J. Immunol.* **174,** 4345–4355
9. Levy, B. D., De Sanctis, G. T., Devchand, P. R., Kim, E., Ackerman, K., Schmidt, B. A., Szczeklik, W., Drazen, J. M., and Serhan, C. N. (2002) *Nat. Med.* **8,** 1018–1023
10. Schmelzer, K. R., Inceoglu, B., Kubala, L., Kim, I. H., Jinks, S. L., Eiserich, J. P., and Hammock, B. D. (2006) *Proc. Natl. Acad. Sci. U.S.A.* **103,** 13646–13651
11. Blaho, V. A., Mitchell, W. J., and Brown, C. R. (2008) *Arthritis Rheum.* **58,** 1485–1495
12. Bafica, A., Scanga, C. A., Serhan, C., Machado, F., White, S., Sher, A., and Aliberti, J. (2005) *J. Clin. Invest.* **115,** 1601–1606
13. Masoodi, M., Mir, A. A., Petasis, N. A., Serhan, C. N., and Nicolaou, A. (2008) *Rapid Commun. Mass Spectrom.* **22,** 75–83
14. Kiss, L., Röder, Y., Bier, J., Weissmann, N., Seeger, W., and Grimminger, F. (2008) *Anal. Bioanal. Chem.* **390,** 697–714
15. Steere, A. C., and Glickstein, L. (2004) *Nat. Rev. Immunol.* **4,** 143–152
16. Barthold, S. W., Beck, D. S., Hansen, G. M., Terwilliger, G. A., and Moody, K. D. (1990) *J. Infect. Dis.* **162,** 133–138
17. Crandall, H., Dunn, D. M., Ma, Y., Wooten, R. M., Zachary, J. F., Weis, J. H., Weiss, R. B., and Weis, J. J. (2006) *J. Immunol.* **177,** 7930–7942
18. Harkewicz, R., Fahy, E., Andreyev, A., and Dennis, E. A. (2007) *J. Biol. Chem.* **282,** 2899–2910
19. Brown, C. R., Blaho, V. A., and Loiacono, C. M. (2003) *J. Immunol.* **171,**

893–901
20. Chen, M., Lam, B. K., Kanaoka, Y., Nigrovic, P. A., Audoly, L. P., Austen, K. F., and Lee, D. M. (2006) *J. Exp. Med.* **203,** 837–842
21. Buczynski, M. W., Stephens, D. L., Bowers-Gentry, R. C., Grkovich, A., Deems, R. A., and Dennis, E. A. (2007) *J. Biol. Chem.* **282,** 22834–22847
22. Deems, R., Buczynski, M. W., Bowers-Gentry, R., Harkewicz, R., and Dennis, E. A. (2007) *Methods Enzymol.* **432,** 59–82
23. Ma, Y., Seiler, K. P., Eichwald, E. J., Weis, J. H., Teuscher, C., and Weis, J. J. (1998) *Infect. Immun.* **66,** 161–168
24. Barthold, S. W., Feng, S., Bockenstedt, L. K., Fikrig, E., and Feen, K. (1997) *Clin. Infect. Dis.* **25,** Suppl. 1, S9–S17
25. Brown, C. R., and Reiner, S. L. (2000) *J. Immunol.* **165,** 1446–1452
26. Chen, M., Boilard, E., Nigrovic, P. A., Clark, P., Xu, D., Fitzgerald, G. A., Audoly, L. P., and Lee, D. M. (2008) *Arthritis Rheum.* **58,** 1354–1365
27. Chizzolini, C., Chicheportiche, R., Alvarez, M., de Rham, C., Roux-Lombard, P., Ferrari-Lacraz, S., and Dayer, J. M. (2008) *Blood* **112,** 3696–3703
28. Straus, D. S., Pascual, G., Li, M., Welch, J. S., Ricote, M., Hsiang, C. H., Sengchanthalangsy, L. L., Ghosh, G., and Glass, C. K. (2000) *Proc. Natl. Acad. Sci. U.S.A.* **97,** 4844–4849
29. Lawrence, T., Willoughby, D. A., and Gilroy, D. W. (2002) *Nat. Rev. Immunol.* **2,** 787–795
30. Powell, W. S. (2003) *J. Clin. Invest.* **112,** 828–830
31. Wertheim, W. A., Kunkel, S. L., Standiford, T. J., Burdick, M. D., Becker, F. S., Wilke, C. A., Gilbert, A. R., and Strieter, R. M. (1993) *J. Immunol.* **151,** 2166–2175
32. Wang, D., Wang, H., Brown, J., Daikoku, T., Ning, W., Shi, Q., Richmond, A., Strieter, R., Dey, S. K., and DuBois, R. N. (2006) *J. Exp. Med.* **203,** 941–951
33. Krause, P., Bruckner, M., Uermosi, C., Singer, E., Groettrup, M., and Legler, D. F. (2009) *Blood* **113,** 2451–2460
34. Michaelis, U. R., and Fleming, I. (2006) *Pharmacol. Ther.* **111,** 584–595
35. Node, K., Huo, Y., Ruan, X., Yang, B., Spiecker, M., Ley, K., Zeldin, D. C., and Liao, J. K. (1999) *Science* **285,** 1276–1279
36. Liu, Y., Zhang, Y., Schmelzer, K., Lee, T. S., Fang, X., Zhu, Y., Spector, A. A., Gill, S., Morisseau, C., Hammock, B. D., and Shyy, J. Y. (2005) *Proc. Natl. Acad. Sci. U.S.A.* **102,** 16747–16752
37. Morisseau, C., and Hammock, B. D. (2005) *Annu. Rev. Pharmacol. Toxicol.* **45,** 311–333
38. Zeldin, D. C., Wei, S., Falck, J. R., Hammock, B. D., Snapper, J. R., and Capdevila, J. H. (1995) *Arch. Biochem. Biophys.* **316,** 443–451
39. Kühn, H., and O'Donnell, V. B. (2006) *Prog. Lipid Res.* **45,** 334–356
40. Murphy, R. C., and Gijón, M. A. (2007) *Biochem. J.* **405,** 379–395
41. Powell, W. S., and Rokach, J. (2005) *Prog. Lipid Res.* **44,** 154–183
42. Wen, Y., Gu, J., Chakrabarti, S. K., Aylor, K., Marshall, J., Takahashi, Y., Yoshimoto, T., and Nadler, J. L. (2007) *Endocrinology* **148,** 1313–1322
43. Dioszeghy, V., Rosas, M., Maskrey, B. H., Colmont, C., Topley, N., Chaitidis, P., Kühn, H., Jones, S. A., Taylor, P. R., and O'Donnell, V. B. (2008) *J. Immunol.* **181,** 6514–6524
44. Wen, Y., Gu, J., Vandenhoff, G. E., Liu, X., and Nadler, J. L. (2008) *Am. J. Physiol. Heart Circ. Physiol.* **294,** H1933–H1938
45. Bolick, D. T., Orr, A. W., Whetzel, A., Srinivasan, S., Hatley, M. E., Schwartz, M. A., and Hedrick, C. C. (2005) *Arterioscler. Thromb. Vasc. Biol.* **25,** 2301–2307
46. McCormick, B. A., Parkos, C. A., Colgan, S. P., Carnes, D. K., and Madara, J. L. (1998) *J. Immunol.* **160,** 455–466
47. Jankov, R. P., Luo, X., Demin, P., Aslam, R., Hannam, V., Tanswell, A. K., and Pace-Asciak, C. R. (2002) *J. Pharmacol. Exp. Ther.* **301,** 435–440
48. McCormick, B. A. (2007) *FEBS J.* **274,** 3513–3518
49. Folco, G., and Murphy, R. C. (2006) *Pharmacol. Rev.* **58,** 375–388
50. Schwab, J. M., Chiang, N., Arita, M., and Serhan, C. N. (2007) *Nature* **447,** 869–874
51. Aliberti, J., Serhan, C., and Sher, A. (2002) *J. Exp. Med.* **196,** 1253–1262
52. Serhan, C. N., Gotlinger, K., Hong, S., Lu, Y., Siegelman, J., Baer, T., Yang, R., Colgan, S. P., and Petasis, N. A. (2006) *J. Immunol.* **176,** 1848–1859
53. González-Périz, A., Planagumà, A., Gronert, K., Miquel, R., López-Parra, M., Titos, E., Horrillo, R., Ferré, N., Deulofeu, R., Arroyo, V., Rodés, J., and Clària, J. (2006) *FASEB J.* **20,** 2537–2539
54. Hayakawa, M., Sugiyama, S., Takamura, T., Yokoo, K., Iwata, M., Suzuki, K., Taki, F., Takahashi, S., and Ozawa, T. (1986) *Biochem. Biophys. Res. Commun.* **137,** 424–430
55. Moghaddam, M. F., Grant, D. F., Cheek, J. M., Greene, J. F., Williamson, K. C., and Hammock, B. D. (1997) *Nat. Med.* **3,** 562–566
56. Itoh, T., Fairall, L., Amin, K., Inaba, Y., Szanto, A., Balint, B. L., Nagy, L., Yamamoto, K., and Schwabe, J. W. (2008) *Nat. Struct. Mol. Biol.* **15,** 924–931
57. Ohta, A., Mayo, M. C., Kramer, N., and Lands, W. E. (1990) *Lipids.* **25,** 742–747
58. Myers, L. K., Kang, A. H., Postlethwaite, A. E., Rosloniec, E. F., Morham, S. G., Shlopov, B. V., Goorha, S., and Ballou, L. R. (2000) *Arthritis Rheum.* **43,** 2687–2693
59. Woods, J. M., Mogollon, A., Amin, M. A., Martinez, R. J., and Koch, A. E. (2003) *Exp. Mol. Pathol.* **74,** 282–290
60. Marcouiller, P., Pelletier, J. P., Guévremont, M., Martel-Pelletier, J., Ranger, P., Laufer, S., and Reboul, P. (2005) *J. Rheumatol.* **32,** 704–712
61. Mao, J. T., Tsu, I. H., Dubinett, S. M., Adams, B., Sarafian, T., Baratelli, F., Roth, M. D., and Serio, K. J. (2004) *Clin. Cancer Res.* **10,** 6872–6878
62. Hong, S., Porter, T. F., Lu, Y., Oh, S. F., Pillai, P. S., and Serhan, C. N. (2008) *J. Immunol.* **180,** 3512–3519
63. Paigen, B., Ishida, B. Y., Verstuyft, J., Winters, R. B., and Albee, D. (1990) *Arteriosclerosis.* **10,** 316–323
64. Wilson, K. R., Napper, J. M., Denvir, J., Sollars, V. E., and Yu, H. D. (2007) *Microbiology* **153,** 968–979
65. Binstadt, B. A., Patel, P. R., Alencar, H., Nigrovic, P. A., Lee, D. M., Mahmood, U., Weissleder, R., Mathis, D., and Benoist, C. (2006) *Nat. Immunol.* **7,** 284–292
66. Sotiriou, C., and Piccart, M. J. (2007) *Nat. Rev. Cancer* **7,** 545–553